Atomistic Modelling and Simulation of Transmission Electron Microscopy Images: Application to Intrinsic Defects of Graphene

Cyril Guedj[1], Léonard Jaillet[2], François Rousse[2] and Stéphane Redon[2]
[1]*Univ. Grenoble Alpes, CEA, LETI, 38000 Grenoble, France*
[2]*Univ. Grenoble Alpes, Inria, CNRS, Grenoble INP*, LJK, 38000 Grenoble, France*
[*]*Institute of Engineering Univ. Grenoble Alpes*

https://www.minatec.org/fr, http://www.leti-cea.fr/cea-tech/leti, https://www.samson-connect.net

Keywords: Atomistic, Atomic, Modelling, Electron Microscopy, STEM, TEM, Microscopy, Graphene, Defects, Vacancy, Microstructure, Image, Simulation, Materials, Characterization, Brenner, Samson.

Abstract: The characterization of advanced materials and devices in the nanometer range requires complex tools, and the data analysis at the atomic level is required to understand the precise links between structure and properties. This paper demonstrates that the atomic-scale modelling of graphene-based defects may be performed efficiently for various structural arrangements using the Brenner module of the SAMSON software platform. The signatures of all kinds of defects are computed in terms of energy and scanning transmission electron microscopy simulated images. The results are in good agreement with all theoretical and experimental data available. This original methodology is an excellent compromise between the speed and the precision required by the semiconductor industry and opens the possibility of realistic *in-silico* research conjugated to experimental nanocharacterisation of these promising materials.

1 INTRODUCTION

Digitals tools are more and more required to study, design and prototype nano-objects, although the underlying physics is so complex that the quest for a universal tool is still far from being over. With the increase of the computational power and the improvement of the simulation methods, new possibilities are offered by these tools and even more shall be expected in the future. The increasing pace of the semiconductor industry requires rapid and efficient simulation and modelling strategies to analyse the results and improve the technological performances of various nano-devices, sensors or actuators. In many systems, the optical or electronic properties are driven by interfacial or by defect-engineered phenomena. In order to understand the links between structure and properties, the nanocharacterisation of materials and devices is advantageously combined with atomistic modelling studies. The equilibrium positions of all atoms provide the necessary basis to simulate the relevant physical properties, which are measured with increasing precision and sensitivity. The combination of experiments conducted in parallel of simulations is particularly relevant in the field of transmission electron microscopy (TEM), because the correlation between the measured image and the actual arrangement of atoms is not straightforward in general. Like most characterizations (TEM, X-ray or electron diffraction, spectroscopic ellipsometry, scanning tunnelling microscopy, etc.), the precise simulation of TEM images is usually mandatory to interpret the experimental results at the atomic scale. With developments in aberration-corrected transmission electron microscopy, it is now possible to characterize vacancy defects in graphene (Novoselov et al., 2004) at atomic resolution, enabling the direct comparison between theoretically predicted structures and experiment. This paper provides an optimised methodology to perform atomic-scale modelling of high resolution scanning transmission electron microscopy (HRSTEM) experiments of graphene-based defects. For this, it uses relaxed structural models obtained with the Brenner module of the Software for Adaptative Modeling and Simulation Of Nanosystems (SAMSON) developed by the NANO-D group at INRIA (www.samson-connect fr). The case of graphene-based defects is extremely interesting,

Guedj C., Jaillet L., Rousse F. and Redon S.
Atomistic Modelling and Simulation of Transmission Electron Microscopy Images: Application to Intrinsic Defects of Graphene.
DOI: 10.5220/0006829200150024
In *Proceedings of 8th International Conference on Simulation and Modeling Methodologies, Technologies and Applications (SIMULTECH 2018)*, pages 15-24
ISBN: 978-989-758-323-0

because this is a 2D material with outstanding mechanical (Geim and Novoselov, 2007), (Lee et al., 2008), (Chen et al., 2008), (Pei et al., 2010), (Scarpa et al., 2009), and electronic (Park et al., 2012); (Lee et al., 2010) properties. Hence, graphene belongs to a family of 2D materials which generates huge expectations in terms of possible applications (Allen and Kichambare, 2007), (Sorkin and Zhang, 2011) (Qureshi et al., 2009), (Joh et al., 2013), (Yao et al., 2009), (Stankovich et al., 2006). The high mobility of graphene makes it advantageous in the perspective of post-silicon electronics, but the defectivity remains a recurrent critical issue. A wide variety of deviations from a perfect crystal might occur during the processing of graphene, either due to the growth conditions or to various sources of degradation, such as knock-on interactions, electron or ionic collisions, plasma damage, chemical reactions, etc. The link between the defectivity and the electronic, magnetic, optical and mechanical properties is critical for the device performance. Thus, the defect engineering is certainly the key of the possible industrial viability of this material. In this paper, we study the defects in graphene in terms of structure and energy. The methodology used to build the systems and to simulate TEM images is explained before presenting simulated graphene-based defects that are compared to available data from the literature.

2 METHODOLOGY

Many methods exist to simulate hydrocarbon systems, such as molecular dynamics, Monte Carlo and the many proposed variants of these approaches. Typically, these simulations come with *ab-initio* quantum-chemistry computations. Therefore, computational studies of complex defects in graphene are often limited by a number of atoms larger than the current first-principle methods can handle. In all cases, these methods require an initial structural model consisting in the description of all atoms in terms of position and chemical nature. In the case of pure crystals, the 3D periodicity helps in calculating all the atom positions for large systems (i.e. more than 50 000 atoms), but in case of localised asymmetrical defects, this task is much more tedious or even completely unfeasible in the worst cases. Hence, a computational tool that is fast enough to handle physically-relevant calculations with tens of thousands atoms is highly desirable. The SAMSON platform and its Brenner module appear to be ideally suited to this task, since they can handle complex models and simulate big systems in a timescale typically less than a day, which is compatible with the feedback delay required by most research teams in nanomaterial characterization. This module appears as an interactive tool for performing predictive modelling, particularly adapted to the very sustained pace of experimentalists and convenient to use, as it is embedded in a user-friendly software platform.

2.1 SAMSON Software

SAMSON is a software platform for computational nanoscience developed by the NANO-D group at Inria and distributed on SAMSON Connect at https://www.samson-connect.net. SAMSON has an open architecture, and users customize their installation with *SAMSON Elements*, i.e. modules for SAMSON that may contain apps, editors, builders, force fields, optimizers, visualizations, etc.

SAMSON Elements are developed with a provided Software Development Kit, and distributed on SAMSON Connect as well.

At the time of writing, about fifty SAMSON Elements are available on SAMSON Connect, for a number of application domains, including materials science (e.g. Brenner model, graphene generator, Universal Force Field, Crystal creator, graphene TEM image analyser, etc.) and drug design (GROMACS force fields, AutoDock Vina, Interactive Ramachandran plots, Normal Modes Analysis, PEPSI-SAXS, etc.).

Users may mix and match SAMSON Elements to design their own processes and workflows, and may use Python scripting to perform modelling and simulation tasks.

2.2 Brenner Model

To simulate the structure of defects in graphene, the atomic positions are computed from energy minimization using the well-known bond-order Brenner interatomic potential (Brenner, 1990), (Brenner, 2000), (Brenner et al., 2002), (Dyson and Smith, 1996), (Los and Fasolino, 2003), (Stuart, et al., 2000), (Brenner et al., 1996). This is a parametrized version of Tersoff's potential which includes terms to correct for the overbindings of radicals. Brenner potential is ideally suited to the interactive digital modelling (virtual nano-engineering) of complex hydrocarbon structures like carbon nanotubes (Sinnott et al., 1999), fullerene (Brenner et al., 1991), or defective single layered graphene (Lehtinen et al., 2010). We detail below

how the energy and forced can be described from this potential.

2.2.1 Energy

The Brenner interatomic potential is particular in the sense that it mostly focuses on covalent bonds (i.e. it does not consider long-range interaction). Therefore the potential energy V_B of the bonding interactions is a sum over interacting atoms (i.e. separated by less than 0.2 nm):

$$V_B = \sum_i \sum_{j>i} [V^R(r_{ij}) - b_{ij} V^A(r_{ij})] \quad (1)$$

The details are given in the original reference (Brenner et al., 2002). Since bonds are defined dynamically via a bond-order function evolving with the interatomic distances, this potential has the ability to describe chemical reactions: it is reactive.

The potential also includes angular and dihedral terms, radical energetics and the influence of π bonds (Bosson et al., 2012).

To overcome the lack of long-range interactions, a non-bonded interaction potential term is added. It consists in a sum of pairwise potential contributions. For simplicity, the approach of Los and Fasolino is chosen (Los and Fasolino, 2002) and the Van der Waals potential term is added:

$$V_{NB}(r_{ij}) = b\ exp(-c_0\ r) - \epsilon\ \left(\frac{\sigma}{r}\right)^6 - V_{shift} \quad (2)$$

to adjust the precision, using b=3224.9 eV, c_0 = 35.995 nm^{-1} , ϵ=0.01396 eV and σ=0.344 nm.

2.2.2 Forces

The force terms can be calculated from the gradient of the potential V. More specifically, the Force F_i applied on atom i at position x_i can be written:

$$F_i = -\frac{\partial V}{dx_i} = -\sum_{j,(i,j)\in\beta} \left(\frac{\partial V}{dr_{ij}}\right)\left(\frac{\partial r_{ji}}{dx_i}\right) \quad (3)$$

where r_{ij} is the distance between atoms i and j, and β is the set of all pairs of atoms involved in the interaction:

$$\beta = \{(i,j), r_{ij} < D_{ij}^{max}\} \quad (4)$$

with D_{ij}^{max} being a threshold distance depending on the atom types.

2.2.3 Adaptive Brenner

An adaptive version of the Brenner potential has been implemented in SAMSON (Bosson et al., 2012). Its interest is that it relies on an algorithm which incrementally updates the forces and the total potential energy.

It basically consists in an incremental dynamical update of the set of interacting atoms and all information related to one, two, three or four atoms. Bonds are divided into 4 types: bond with a relative motion, bonds with a change in potential, bond with a change in conjugate number, and bonds without any change in potential. After initialization, all terms with relative motions are updated incrementally and after a first level and second level potential update, the forces are henceforward updated. This allows the algorithm to linearly scale with the number of updated bonds. Therefore the computational cost is decoupled from the number of atoms in the system and physically-based editing becomes markedly faster.

To take advantage of adaptive Brenner, an adaptive mechanism is proposed in SAMSON to update when minimizing a system. Such an approach in Cartesian coordinates consists in deciding for each atom if it might move or be frozen in space. This decision is made by comparing the norm of its potential displacement with a threshold value, either automatically deduced from the system state or by a manual choice fixed by the user. This implementation is an extension of the internal coordinates and articulated bodies simulation (Redon et al., 2005).

This efficient update mechanism allows continuous minimization of the system energy during the edition of the system, which helps to build realistic structures in a very convenient manner. The user action step (creating/moving/deleting atoms) alternates with the adaptative minimization steps to parallelize the structure editing and the energy minimization.

2.3 Simulation of Microscopy Images

Once the structure is fully relaxed, it is possible to compute the corresponding high-resolution scanning transmission microscopy image by using the QSTEM software (Koch, 2002). This program allows accurate image simulations including fully dynamic calculations. QSTEM computes the true 3D potential distribution and numerically integrates every slice of the potential map. This enables a thickness reduction without limitations in the multislice calculation. In addition, it is possible to explore a wide range of experimental setups in order to evaluate the best conditions to observe the defects. Here the images are simulated using a

typical voltage of 80 kV, a C3 spherical aberration of 0.001 mm, a Cc chromatic aberration of 1 mm, an energy spread of 0.16 eV and a convergence angle of 20 mrad, which are reasonable values to compare with high-resolution scanning transmission electron microscopy (HRSTEM) experiments from an aberration-corrected microscope. The detectors collection angle are chosen between 50 mrad and 200 mrad for realistic high-angle annular dark field (HAADF) conditions. In this conditions of Z-contrast imaging, the contrast scales with the atomic number with a power-law dependence (Crewe et al., 1970). In addition, the HRTEM images are also calculated with QSTEM using a voltage of 80 kV, all aberration coefficients equals to zero except for the chromatic aberration of 1 mm, a spherical aberration of 5 µm and a vibration of 3 nm in all directions. In these conditions, the HRTEM contrasts are usually comparable to HRSTEM, and the superimposition of the atomic model to the (S)TEM image provides an efficient method of validation. To outlines the most striking features, we have used suitable look-up tables (LUT) to colorize the experimental TEM and the simulated STEM images.

3 RESULTS AND DISCUSSION

In the following, we illustrate the cases of typical defects induced by electron-beam damage during TEM observation. The probability to observe these defects is therefore relatively high, for instance when the electron beam energy is set up above the threshold for knock-on damage in sp^2-bonded carbon structures (i.e. > 100 keV) (Banhart et al., 1999), (Smith et al., 2001). These defects could also be obtained by other interactions, such as ionic or mechanical or by plasma damage, for instance if the technological processing steps are inappropriate. We focus the analysis on simple topological defects, vacancies and adatom, but the same conclusion applies to all defects we have studied so far (dislocations, novel phases, extended defects, etc.), based on available published data.

In the following figures, colorization of experimental images is obtained with Fiji (Schindelin et al., 2012) using 16 colors LUT. The various atomistic models correspond to flake system of 1308 atoms with flat borders, built in SAMSON and optimized thanks to the Brenner module. The clear advantage of the Brenner approach compared to ab-initio is a ~ 4 orders of magnitude improvement in terms of simulation speed. Moreover, as we will see, the precision achieved is sufficient to match the experimental results and we obtained similar findings for all the graphene-based defects we found in literature, without apparent limitation, and even for systems with tens of thousands of atoms. In the following, all experimental data already published are used with permissions.

3.1 Stone-Wales Defect

Graphene has the ability to form nonhexagonal rings, and the simplest example is the Stone-Wales (SW) defect (Stone et al., 1986) in which four hexagons are transformed into two pentagons and two heptagons [SW(55-77) defect] by an in-plane 90° rotation of two carbon atoms with respect to the midpoint of the C-C bond (Figure 1).

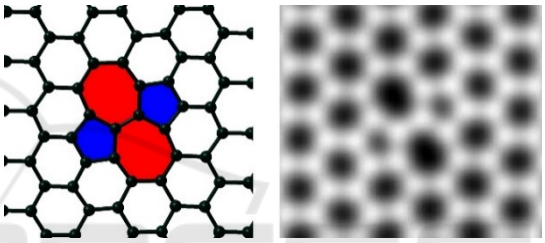

Figure 1: Left: atomistic ball and stick model of the unstable flat SW(55-77) defect in graphene. Black balls represent carbon atoms. Right: Corresponding HRSTEM-HAADF simulated image.

In pure graphene, the C-C bond distance is 0.142 nm according to Pauling (Pauling, 1960), which is the exact value provided by our code. The simulation also matches very well previous experimental results (Meyer et al., 2008), (Kotakoski et al., 2011) and the corresponding *ab-initio* simulations (Li et al., 2005), (Ma et al., 2009).

The planar configuration is unstable and may relax in the 3D sinelike or cosinelike configuration. In our case, the minimum energy configuration of 6 eV is obtained for the sinelike configuration (Figure 2), in reasonable agreement with the configuration and the energy of 5.82 ± 0.03 eV obtained by quantum Monte Carlo (Ma 2009) and the value of 5.9 eV obtained by DFT-LDA (Jensen et al., 2002).

An absolute comparison with the exact and precise value of the formation energy is difficult because of the significant dispersion of formation energies published in the literature, depending on the DFT options (LDA, GGA, PW91, PBE, PBE0, B3LYP, M06-L, vdW-DF, DFT-D, etc.) or the size of the supercell for instance (Ma et al., 2009), (Li et al., 2005), (Zhang et al., 2016), (Trevethan et al.,

2014), (Skowron et al., 2015). Meanwhile, the buckling height value of 0.156 nm is very close to the value of 0.161 nm obtained by DFT for the biggest cell (11 x 11) of Ma et al. (Ma et al., 2009). The SW defects are not simple planar defects but rather involve 3D displacements. Our simulation provides realistic 3D positions of all atoms from a 2D TEM image.

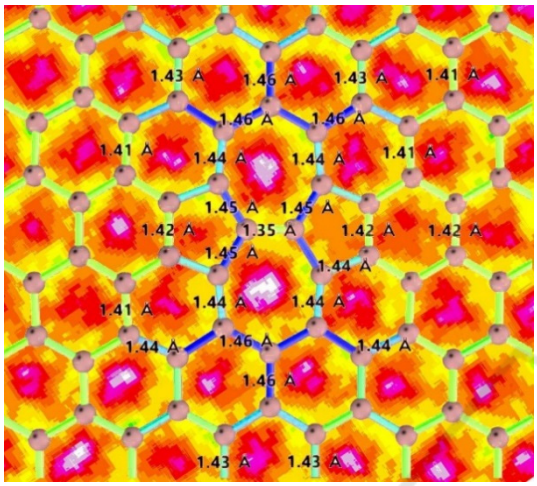

Figure 2: Atomistic model of the lowest energy configuration SW(55-77) sinelike defect in graphene, with bond distances, superimposed with the experimental HRTEM image of Kotakoski (Kotakoski et al., 2011). Colorization has been added to help the interpretation.

3.2 Monovacancy (V_1 Defects)

3.2.1 Case V_1 (5-9)

The removal of one carbon atom from the graphene network results in the formation of a single vacancy, which has been studied both theoretically and experimentally (Ma et al., 2009), (Li et al., 2005), (Kotakoski et al., 2011), (Gass et al., 2008), (Meyer et al., 2008), (Girit, 2009).

Our simulated model matches precisely the experimental HRTEM images published in the literature (Figure 3, Figure 4 and Figure 5). We obtained a formation energy of 5.45 eV, which is less than the range of [7.6, 7.9] eV obtained by DFT (Skowron et al., 2015). The symmetric monovacancy (s-MV) is known to exhibit a Jahn Teller distortion, and may reconstruct into a closed five- and nine-membered pair of rings. The reconstructed monovacancy (r-MV) arrangement lowers the energy of the symmetrical vacancy structure in agreement with *ab-initio* calculations (El-Barbary et al., 2003).

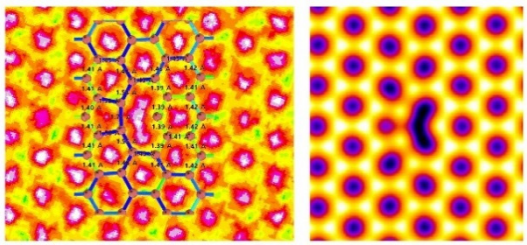

Figure 3: Left: atomistic model of the V_1 (5-9) defect superimposed to the colorized experimental HRTEM image (Kotakoski et al., 2011). Right: simulated HRSTEM-HAADF image.

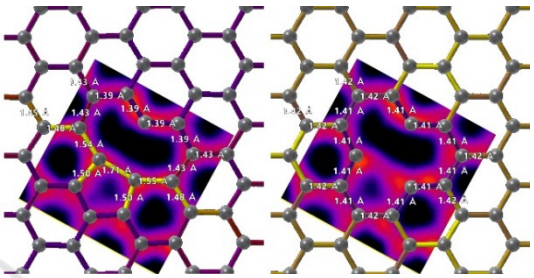

Figure 4: Atomistic model of the V_1 (5-9) defect superimposed to the experimental HRTEM image published by Robertson (Robertson 2013). Left: r-MV (also labelled C_{2v}). Right: s-MV (also labelled D_{3h}).

Another comparison with HRTEM experiment (Figure 4) shows that the best agreement between experiment and simulation is obtained for the reconstructed model r-MV, in expected agreement with our lowest computed energy. Hence, our methodology provides a convenient and realistic approach to model the HRTEM images at the atomic scale for this case.

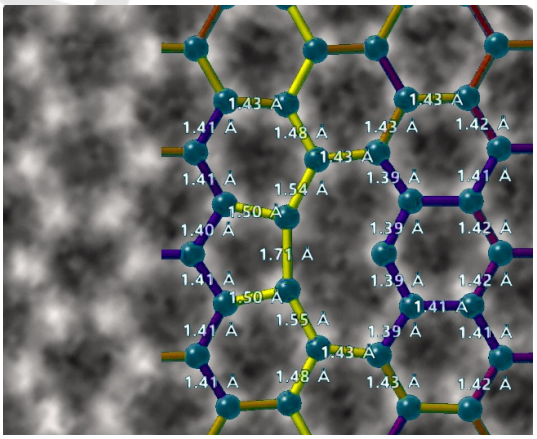

Figure 5: Atomistic model of the V_1 (5-9) defect r-MV superimposed to the experimental HRTEM defect image entitled "SALVE-III-project-HRTEM-graphene-vacance-foreign-atoms-defects-zoom.png" obtained by the SALVE III project (Salve, 2018).

We found similar findings for all the cases we have studied, without any exception. In general, the precise comparison with experiment must include the possible extrinsic contamination by oxycarboneous species, by hydrogen or by water for instance to be fully significant, therefore a relevant comparison should take all these effects into account.

3.2.2 Case V_1 (5-5)

The V_1 (5-5) state (Figure 6) may be considered as intermediary between the V_1 (5-9) r-MV and s-MV (Trevethan et al., 2014). Our calculations predicts a formation energy of 5.01 eV, which means that such defect should be observable in principle.

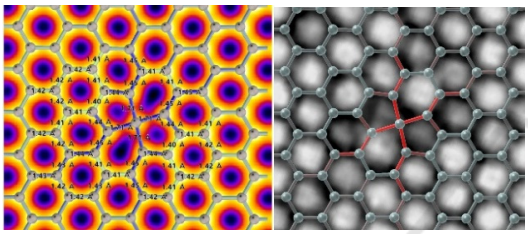

Figure 6: Left: atomistic model of the V_1 (5-5) defect superimposed to the simulated HRSTEM image. Right: model superimposed to the experimental HRSTEM image (Lehtinen et al., 2013).

The simulated HRSTEM-HAADF of Figure 6 is so close to the image of pure graphene that it might not be identified in most cases, except perhaps in ultra-low doses quantitative experiments to minimize the knock-on energy provided by the incident electrons and at very low temperatures to freeze the thermal motion. In the supplementary movie provided by Lehtinen (Lehtinen et al., 2013), a pattern similar to the V_1 (5-5) is possibly obtained, just prior to the formation of a more extended defect. Although the contrasts are very rapidly changing, the V_1 (5-5) is presumably a reactive seed for more complex defect growth.

This type of defect has been observed experimentally with the central 4-fold atom being substituted by silicon (Ramasse et al., 2013).

3.3 Divacancy (V_2 Defects)

3.3.1 Case V_2 (5-8-5)

When two individual diffusing mono-vacancies meet they will coalesce into a nearest-neighbour di-vacancy defect (equivalent to removing a carbon dimer from the lattice). This process results in the formation of the stable pentagon–octagon– pentagon (5–8–5) structure, which has been widely observed in high-resolution transmission electron microscopy (HRTEM) images (Kotakoski et al., 2011), (Warner et al., 2012), (Lehtinen et al., 2013) (Robertson and Warner 2013). Our calculation provides a formation energy of 7.29 eV, not far from 7.59 eV by DT-LDA (Saito et al., 2007) and 7.52 eV by Tight Binding (Xu et al., 1993), (Dettori et al., 2012).

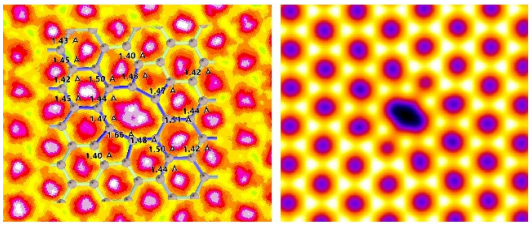

Figure 7: Left: atomistic model of the V1 (5-8-5) defect superimposed to the colorized experimental HRTEM image (Kotakoski et al., 2011). Right: simulated HRSTEM-HAADF image.

The comparison with experiment (Figure 7) is once again very positive, with a nearly perfect match with published experimental TEM results.

The V_2 (5-8-5) defects may mutate into the V_2 (555-777) and V_2 (5555-6-7777) states due to electron beam irradiation for instance, and these transitions were observed by HRTEM (Robertson, 2012), (Kotakoski et al., PRL 2011), (Kotakoski et al., PRB 2011).

3.3.2 Case V_2 (555-777)

The structure of the V_2 (555-777) divacancy is displayed in Figure 8, showing an excellent agreement between experiment and simulation.

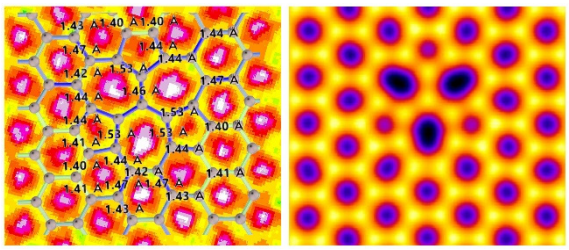

Figure 8: Left: atomistic model of the V_1 (555-777) defect superimposed to the colorized experimental HRTEM image (Kotakoski et al. 2011). Right: simulated HRSTEM-HAADF image.

The calculated formation energy is 7.14 eV, in reasonable agreement with the value of 7.41 eV obtained by DFT-PBE/DNP (Wu et al., 2013).

Hence the V_2 (555-777) state should be more stable than the V_2 (5-8-5), in agreement with all DFT results published (Skowron et al., 2015).

3.3.3 Case V_2 (5555-6-7777)

The divacancy state V_2 (5555-6-7777) is represented in Figure 9, superimposed to the experimental HRTEM image attributed to this defect by Kotakoski. Surprisingly, the matching is not perfect and the TEM image appears asymmetrical as opposed to the simulated image.

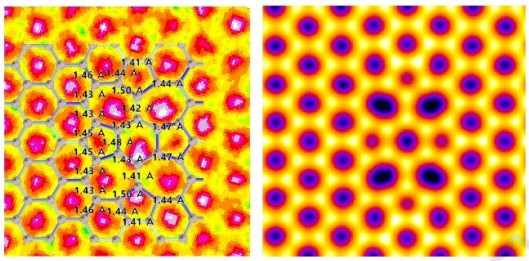

Figure 9: Left: atomistic model of the V_2 (5555-6-7777) defect superimposed to the colorized experimental HRTEM image (Kotakoski et al., 2011). Right: simulated HRSTEM-HAADF image.

The computed formation energy is 7.45 eV, close to the DFT value of 7.08 eV (Wu et al., 2013). According to our simulation, this defect should be less stable than the V_2 (5-8-5), whereas Wu predicts the opposite conclusion.

To understand this apparent contradiction, we have tried to obtain a better match to the experimental results, because we believe that ultimately Nature is never wrong. This corresponds to the trivacancy case as reported below.

3.4 Trivacancy (V_3 Defects)

3.4.1 Case V_3 (5555-666-77)

A set of studies is devoted to the structure and energetics of trivacancies in graphene obtained by structure reconstruction rearrangements after removing 3 carbon atoms (Dai et al., 2011), (Faccio et al., 2012), (Saito et al., 2007). Experimentally, the trivacancy state may be obtained for instance by bombardment with energetic particles (Wang et al., 2012). The V_3 (5555-666-77) structure has not been studied to our knowledge, yet it apparently provides the best agreement (Figure 10) with the experimental image tentatively attributed to the V_2 (5555-6-7777) by Kotakoski et al., (2011).

This novel defect structure has a formation energy of 12.54 eV. We therefore suggest that this trivacancy may occur during e-beam irradiation. This case highlights particularly well the interest of our methodology which offers a new way to explore *in-silico* novel types of defects, perhaps unpublished, and yet observed experimentally by HRTEM or HRSTEM.

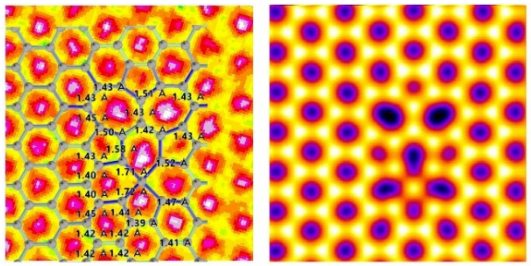

Figure 10: Left: atomistic model of the V3 (5555-666-77) defect superimposed to the colorized experimental HRTEM image tentatively attributed to the V2 (55555-6-7777) defect (Kotakoski et al., 2011). Right: simulated HRSTEM-HAADF image.

3.5 Carbon Adatom

The healing (self-repair) of various graphene defects by migration of adatoms has been observed by HRTEM (Song et al., 2011), (Robertson et al., 2012). The result of our calculation is displayed in Figure 11.

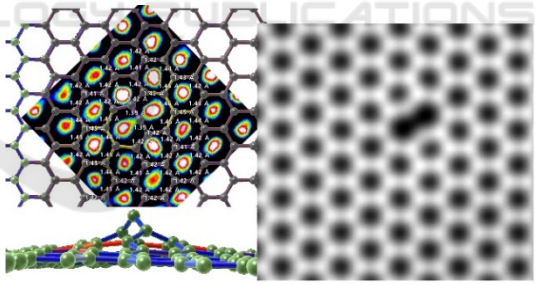

Figure 11: Left: atomistic model of the 1C adatom defect superimposed to the colorized experimental HRTEM image extracted from the supplementary movie 6 provided in (Lehtinen et al., 2013). Right: corresponding simulated HRSTEM-HAADF image.

DFT studies usually gives three stable positions of the adatom on graphene (Tsetserisa and Pantelides, 2009). The bridge position is predicted to be the most stable and was observed by HRTEM (Hashimoto et al., 2004) and by HRSTEM (Bangert et al., 2009). We obtain a formation energy of 2.69 eV, therefore such defect should form easily during processing of a graphene-based nanodevice. The DFT method provides a value of the order of 1.5-2

eV for the binding energy of the carbon adatom (Lee et al., 1997); (Lehtinen et al., 2003). The perpendicular distance of the adatom to the graphite surface is ~ 0.222 nm, not too far from the value of 0.187 nm previously obtained by ab-initio calculations for 50 atoms (Lehtinen et al., 2003). In our case, we find that the 5th nearest neighbours around the carbon adatom are vertically displaced, therefore a simulation box of 50 atoms is certainly too small to simulate the full relaxation of the structure. Indeed, we obtained that 192 atoms are vertically displaced by more than 0.005 nm around the carbon adatom. Our methodology therefore provides extended strains and stresses over long distances, which is not possible with other methods restricted to a limited number of atoms.

3.6 Extended Edge Defect (88-7-5555)

A severe test to assess the validity of a structural model consists in considering a complex defective structure with a large number of atoms. Hence, we have used an extended defect and the excellent spatial resolution obtained by the Salve project (Salve, 2018) to check our methodology. The double correction of chromatic and spherical aberrations provides information transfer until 71 pm, which is probably the best result ever obtained for an image of graphene. The comparison is depicted in Figure 12. As usual, a nearly perfect agreement between simulation and experiment is obtained.

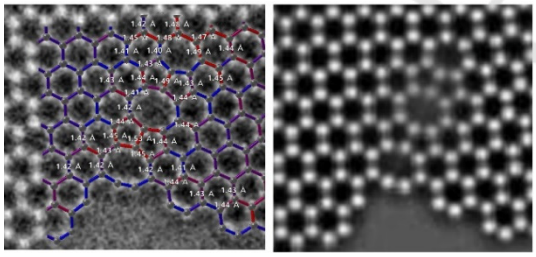

Figure 12: Left: atomistic model of the extended defect 88-7-5555 defect superimposed to the experimental HRTEM image entitled "SALVE-III-project-HRTEM-graphene-vacancy-characteristic-defects.png" (Salve, 2018). Right: corresponding simulated HRTEM image.

The simulation also provides the distortion maps for all bonds, in 3D and with picometric spatial resolution. The positions of all atoms in the system are therefore extracted and are readily available for further *ab-initio* calculations in order to get all the physical properties (electronic, optical, mechanical, magnetic, etc.).

4 CONCLUSIONS

Using the Brenner module of the SAMSON platform, we have precisely matched the experimental high resolution transmission electron microscopy experiments of various graphene-based defects. We have also shown that a good agreement is obtained with more complex ab-initio simulations in terms of structure and energy. This methodology opens the pathway to more extensive *in-silico* exploration of all forms of phases or defects in carbon-based materials, like diamond-like carbon (DLC), amorphous carbon, nanotubes, fullerenes, pentaheptite (Crespi et al., 1996), or other novel phases or defects. Apparently, there is virtually no limit in the number of structural arrangements of graphene-based defects that can be simulated with the Brenner module of SAMSON, in good matching with experimental results. Finally, this methodology is therefore a reliable approach to obtain 3D atomistic models from 2D experimental TEM images.

In the future, we would like to extend such a methodology to study in detail the possible transitions between different types of defects.

ACKNOWLEDGEMENTS

The invaluable contribution from the platform of nanocharacterization (PFNC) at MINATEC, Grenoble, France is respectfully acknowledged (https://www minatec.org/en/). We would like to gratefully acknowledge funding from the European Research Council through the ERC Starting Grant No. 307629.

REFERENCES

Allen, B.L. et al., 2007. Carbon nanotube field-effect-transistor-based biosensors, *Adv Mater*, 19 (11), pp. 1439-1451.

Ansari R. et al., 2012. Mechanical properties of defective single-layered graphene sheets via molecular dynamics simulation. *Superlattices and microstructures*, 51, 274-289.

Bangert U. et al., 2009, Nanotopography of graphene, *Phys. Status Solidi A*, 206, 2115–2119.

Banhart F. et al., 1999. Irradiation effects in carbon nanostructures, *Rep. Prog. Phys*. 62, 1181.

Banhart F. et al., 2011, Structural defects in graphene, *ACS Nano*, 5(1), pp 26-41.

Bosson et al., 2012. Interactive physically-based structural modeling of hydrocarbon systems, *J. of Computational Physics*, vol. 231, 6, p 2581-2598.

Brenner D.W. et al., 1996. Simulated engineering of nanostructures, *Fourth Foresight Conference on Molecular Nanotechnology*.

Brenner D.W., 1990. Empirical potential for hydrocarbons for use in simulating the chemical vapor deposition of diamond films, *Phys. Rev. B*, 42, 9458-9471.

Brenner D.W. et al. 1991, Molecular dynamics simulations of the nanometer-scale mechanical properties of compressed

Buckminsterfullerene", *Thin Solid Films* 206, 220–223.

Brenner D.W., 2000. The art and science of an analytic potential, *Phys. Stat. Sol. (b)* 217, 23–40.

Brenner D.W. and al. 2002, A second-generation reactive empirical bond order (REBO) potential energy expression for hydrocarbons, *J. Phys.: Condens. Mater.* 14, 783–802.

Chen H. et al., 2008. Mechanically strong, electrically conductive, and biocompatible graphene paper, *Adv. Mater*. 20 (18), pp 3557-3561.

Crespi V. H. et al., Prediction of a pure-carbon planar covalent metal, Phys. Rev. B 53, R13303(R) (1996)

A. V. Crewe, J. Wall, and J. Langmore, Science 168, 1338 (1970).

Dai X. Q. et al., 2011. First-principle study of magnetism induced by vacancies in graphene, Eur. Phys. J. B, 80, 343–349.

Dettori R. et al. 2012, Elastic fields and moduli in defected graphene, *J. Phys.: Condens. Matter*, 24, 104020.

Dyson A.J. and Smith P.V., 1996. Extension of the Brenner empirical interatomic potential to C–Si-H systems. *Surf. Sci.* 355, 140–150.

El-Barbary A.A. et al., 2003. Structure and energetics of the vacancy in graphite, *Phys. Rev. B* 68, 144107.

Faccio R. et al., 2012. Magnetism in multivacancy graphene systems, *J. Phys.: Condens. Matter,* 24, 375304.

Gass M.H. et al., 2008. Free-Standing Graphene at Atomic Resolution, *Nat. Nanotechnol*, 3, 676–681.

Geim A.K. and Novoselov K.S., 2007. The rise of graphene, *Nat. Mater* 6, pp 183-191.

Girit Ç Ö. Et al., Graphene at the Edge: Stability and Dynamics, Science 27 Mar 2009, Vol. 323, Issue 5922, pp. 1705-1708

Hashimoto A. and al., 2004. Direct evidence for atomic defects in graphene layers, *Nature*, 430, 870–873, DOI: 10.1038/nature02817

Jensen P. and al. 2002. Catalysis of nanotube plasticity under tensile strain, *Phys. Rev. B,* 66, 193403.

Joh H.-I. et al., 2013. Synthesis and properties of an atomically thin carbon nanosheet similar to graphene and its promising use as an organic thin film transistor, *Carbon*, 55, pp. 299-304.

Koch C., 2002. Determination of core structure periodicity and point defect density along dislocations. *PhD. Thesis, Arizona State University.*

Kotakoski J. et al., 2011. From point defects in graphene to two-dimensional amorphous carbon, *Phys. Rev. Lett*. 106, 105505.

Kotakoski J. et al. (2011). Stone-Wales-type transformations in carbon nanostructures driven by electron irradiation, *Phys. Rev. B*, 83, 245420.

Lee C. et al., 2008. Measurement of the elastic properties and intrinsic strength of monolayer graphene, *Science* 321 (5887), pp 385-388.

Lee E. et al., 2010. Electrical properties and photoconductivity of stacked-graphene carbon nanotubes, *Adv Mater*, 22 (16), pp. 1854-1857.

Lee Y.H. et al., 1997. Catalytic Growth of Single-Wall Carbon Nanotubes: An ab Initio Study, *Phys. Rev. Lett.*, 78 2393-2396.

Lehtinen O. et al., 2003. Magnetic Properties and Diffusion of Adatoms on a Graphene Sheet. *Phys. Rev. Lett.*, 91, 017202.

Lehtinen O. et al., 2010. Effect of ion bombardment on a two-dimensional target: atomistic simulations of graphene irradiation, *Phys. Rev. B* 81(15), 153401.

Lehtinen O. et al., 2013. Atomic scale study of the life cycle of a dislocation in graphene from birth to annihilation, *Nat. Commun.,* 4, 3098.

Li L. et al., 2005. Defect energies of graphite: density-functional calculations, *Phys. Rev. B* 72, 184109.

Los J.H. and Fasolino A., 2002. Monte Carlo simulations of carbon-based structures based on an extended Brenner potential, *Comput. Phys. Commun.* 147,

178–181.

Los J.H. and Fasolino A., 2003. Intrinsic long-range bond-order potential for carbon: performance in Monte Carlo simulations of graphitization, *Phys. Rev. B* 68, 024107.

Ma J. et al., 2009. Stone-Wales defects in graphene and other planar sp^2-bonded materials, *Phys. Rev. B* 80, 033407.

Meyer J.C. et al., 2008. Direct imaging of lattice atoms and topological defects in graphene membranes, *Nano Letters*, Vol. 8, nº11, 3582-3586.

Novoselov K.S. et al., 2004. Electric field effect in atomically thin carbon films. *Science* 306.5696: 666-669.

Park S. et al., 2012. The effect of concentration of graphene nanoplatelets on mechanical and electrical properties of reduced graphene oxide papers, *Carbon*, 50 (12), pp. 4573-4578.

Pauling L., 1960. The Nature of the Chemical Bond, *Cornell Univ. Press, NY.*

Pei Q.X. et al., 2010. A molecular dynamics study of the mechanical properties of hydrogen functionalized graphene, *Carbon*, 48 (3), pp 898-904.

Qureshi A. et al., 2009. Review on carbon-derived, solid-state, micro and nano sensors for electrochemical sensing applications. *Diamond and Related Materials*, 18.12, 1401-1420.

Ramasse Q.M. et al., 2013. Probing the Bonding and Electronic Structure of Single Atom Dopants in Graphene with Electron Energy Loss Spectroscopy, *Nano. Lett*., 13, 4989-4995.

Redon S. et al. 2005. Adaptive dynamics of articulated bodies, *ACM Trans. Graph. (TOG)*. Vol. 24, No. 3, pp 936-945.

Robertson A. W. et al. 2012, Spatial control of defect creation in graphene at the nanoscale, *Nat. Commun.*, 3, 1144–1151.

Robertson A. W. and Warner J. H., 2013. Atomic resolution imaging of graphene by transmission electron microscopy, *Nanoscale*, 5, 4079– 4093.

Robertson A. W. et al., 2013. Structural reconstruction of the graphene monovacancy, *ACS nano*, 7(5), 4495–4502.

Saito M. and al., 2007. Magic Numbers of Graphene Multivacancies, *Japanese Journal of Applied Physics*, 46(12L), L1185.

Salve 2018. http://www.salve-project.de/home.html.

Scarpa F. and al., 2009. Effective elastic mechanical properties of single layer graphene sheets, *Nanotechnology*, 20 (6), pp. 1-11.

Schindelin et al., 2012. Fiji: an open-source platform for biological-image analysis, *Nature methods*, 9(7), 676.

Sinnott S.B. et al., 1999. Model of carbon nanotube growth through chemical vapor deposition,

Chem. Phys. Lett. 315, 25–30.

Skowron S. et al., 2015. Energetics of atomic scale structure changes in graphene, *Chem. Soc. Rev.*, 44, 3143.

Smith B.W. et al., 2001. Electron irradiation effects in single wall carbon nanotubes, *J. Appl. Phys.* 90, 3509.

Song B. et al., 2011. Atomic-scale electron-beam sculpting of near-defect-free graphene nanostructures, *Nano Lett.*, 11, 2247–2250.

Sorkin V. and Zhang Y.W., 2011. Graphene-based pressure nano-sensors, *J. Mol. Model*, 17(11), pp. 2825-2830.

Stankovich S. et al., 2006. Graphene-based composite materials, *Nature*, 442 (7100), pp. 282-286.

Stone A.J. et al., 1986. Theoretical Studies of Icosahedral C_{60} and some related species, *Chem. Phys. Lett.*, 128, 501-503.

Stuart S.J. et al., 2000. A reactive potential for hydrocarbons with intermolecular interactions, *J. Chem. Phys.*, 112, 6472.

Trevethan T. et al., 2014. Vacancy diffusion and coalescence in graphene directed by defect strain fields, *Nanoscale*, 6, 2978-2986.

Tsetserisa L. and Pantelides S. T., 2009. Adatom complexes and self-healing mechanisms on graphene and single-wall carbon nanotubes, *Carbon*, 47, 901-908.

Ugeda M.M. et al., 2010. Missing Atom as a Source of Carbon Magnetism, *Phys. Rev. Lett.*, 104, 096804.

Wang H. et al., 2012. Doping Monolayer Graphene with Single Atom Substitutions, *Nano Lett.*, 12, 141-144.

Warner J. H. et al., 2012. Dislocation-driven deformations in graphene, *Science*, 337, 209.

Wu L. et al. 2013. First-principles study on migration and coalescence of point defects in monolayer graphene, *J. Phys. Chem. C*, 117, 17066-17072.

Xu C. H. et al., 1993. Simulations of point-defect properties in graphite by a tight-binding-force model, *Phys. Rev. B.*, 48.18:13273.

Yao J. et al., 2009. In situ chemical synthesis of SnO_2–graphene nanocomposite as anode materials for lithium-ion batteries, *Electrochem Commun*, 11(10), pp. 1849-1852.

Zhang W. et al., 2016. Tight-binding calculation studies of vacancy and adatom defects in graphene, *J. Phys. Condens. Matter 28*, 115001.